Shape transformation from silver triangular nanoprisms to nanodisks: Raman characterization and sculpturing mechanism

I.A. López[a], M. Ceballos[a], G. Hernández[b], L. Acosta[c], and I. Gómez[a]
[a]*Universidad Autónoma de Nuevo León, UANL, Facultad de Ciencias Químicas, Laboratorio de Materiales I, Av. Universidad, Cd. Universitaria 66451, San Nicolás de los Garza, Nuevo León, Mexico.*
[b]*Deparamento de Nanotecnología, Centro de Física Aplicada y Tecnología Avanzada, Universidad Nacional Autónoma de México, Campus Juriquilla, Boulevard Juriquilla No. 3001, 76230, Juriquilla, Querétaro, Mexico.*
e-mail: genoveva@unam.mx
[c]*Escuela Nacional de Estudios Superiores, Universidad Nacional Autónoma de México, Unidad León, Boulevard UNAM No. 2011 Predio el Saucillo y el Potrero 36969, León, Guanajuato, Mexico.*

Received 12 September 2014; accepted 13 January 2015

The sculpturing action of chloride ions on silver nanoplates is investigated. Recent reports show that the shape transformation from silver triangular nanoprisms to nanodisks by addition of chloride ion occurs after a threshold concentration. In this work, a chemical study of this threshold concentration is presented. There is theoretical and experimental evidence that the morphological change only depends on the chloride ion concentration and not on the Cl^-/Ag molar ratio. Besides, the chloride ion etching ability is attributed to the $(AgCl)^\circ$ complex, which controls the morphology change through a stepwise process where a silver atom is removed from the (110) plane, and is subsequently deposited on the (111) plane (i.e. from the nanoplate vertex to the basal plane). The threshold chloride ion concentration in the shape transformation coincides with the point where Ag^+ ion and $(AgCl)^\circ$ concentrations are the same. On the other hand, the quantitative formation of $AgCl_2^-$ avoids the stepwise process, and then the colloidal system is destabilized. Furthermore, the analysis of the Raman spectra supports the transformation mechanisms.

Keywords: Silver triangular nanoprisms; silver nanodisks; Raman spectroscopy.

PACS: 81.07.-b

1. Introduction

Noble metal nanoparticles, as silver and gold, are of great interest because of their unique physical and chemical properties [1-6]. The localized surface plasmon resonance (LSPR) exhibited by these particles allow their potential application as sensors [7,8], optoelectronic materials [9,10], catalysts [11,12] and active substrates for surface-enhanced Raman spectroscopy [13-16]. The LSPR highly depends on the size, shape and surface environment of the metal nanoparticle. Silver and gold nanoparticles have been synthesized with different shapes as spheres [17], rods [18], cubes [19], stars [20], and various other geometries. However, silver nanoparticles undergo morphological changes by different mechanisms that can be roughly divided in three: photoinduced [21], thermal [22] and chemical mechanisms [23]. Similarly, chemical mechanisms can be governed by redox [24], acid-base [25] and solubility-complex [26] equilibria. In this work we are interested in clarifying the morphological transformation of silver nanoprisms into nanodisks by means of solubility-complex equilibria with chloride ions. An et al. [27] reported for the first time the conversion of triangular silver nanoprisms into nanodisks by adding chloride ions into the nanoprisms dispersion. This morphological transformation is attributed to the facet selective etching effect of chloride ions at their vertices due their higher surface energy. Recently, a threshold concentration of chloride ions to initiate the sculpting effect was found by Tang *et al*. [28] and Hsu *et al*. [29]. Below this concentration (3 to 4×10^{-4} M) no morphological change is observed. In this work, we present the Raman characterization and chemical study of this threshold concentration and we explain some results of our own experiments as well as those of other groups.

2. Experimental Section

All chemical reagents used in this work were of analytical grade and were used without any further purification. A Perkin-Elmer lambda 12 spectrophotometer was employed for the UV-Vis analysis of the silver nanoparticle dispersions. For the morphological characterization, the nanoparticles were deposited onto a carbon-coated copper grid and then analyzed by transmission electron microscopy (TEM) using a JEOL JEM-1010 microscope. For the Raman dispersive spectroscopy analysis, the silver dispersions were deposited onto an aluminum support and mounted in the sampling compartment of a Senterra Bruker Raman spectrometer coupled with an Olympus microscope with a 50 X objective; all the samples were analyzed with integration time of 10 s, 6 scans, and laser wavelength and power of 785 nm and 50 mW, respectively.

Silver nanospheres were synthesized by dropwise addition of 1 mL of 8.0 mM $NaBH_4$ solution to 100 mL of a 0.1 mM $AgNO_3$ and 1.5 mM trisodium citrate aqueous solution under vigorous stirring. Silver triangular nanoprisms were obtained via a photoinduced growth method, which was

reported in our previous work [30]. The silver nanosphere dispersion was irradiated by a conventional sodium lamp of 70 W. After 24 h, the colour of the colloid turned blue, which is the characteristic colour of the silver triangular nanoprism dispersions. With the purpose of show the halide concentration effect on the nanoparticle shape, 1 mL of 0.010, 0.10 and 1.0 mM KCl solutions were added into 5 mL of triangular nanoprism dispersion under vigorous stirring. UV-Vis absorption spectra and TEM images of the silver nanoparticles were recorded.

3. Results and Discussion

UV-Vis absorption spectrum of the aqueous dispersion of silver triangular nanoprisms is shown in Fig. 1. The absorption spectrum shows four surface plasmon resonance bands [31], the 331 nm peak is the out-of-plane quadrupole resonance, the 687 nm peak is the in-plane dipole resonance, and the 420-540 nm wide band is the convolution of the out-of-plane dipole and the in-plane quadrupole resonances. This is according with Mie's theory [32], which predicts that anisotropic particles could show two or more surface plasmon resonance bands depending on their shape. Figure 2 shows TEM image of the silver triangular nanoprisms obtained by the photoinduced growth method.

UV-Vis absorption spectra of the aqueous dispersions of silver nanoparticles, obtained by addition of chloride ion solutions of different concentrations, are shown in Fig. 3. The addition of 0.010 or 0.10 mM KCl solutions to the triangular nanoprisms colloidal dispersion causes no significant change in their absorption spectra. On the other hand, the spectrum of the silver colloidal dispersion after the addition of 1.0 mM KCl solution exhibits a large blue-shift to 462 nm of the in-plane dipole plasmon resonance band. Theoretical calculations indicate that the in-plane dipole plasmon resonance

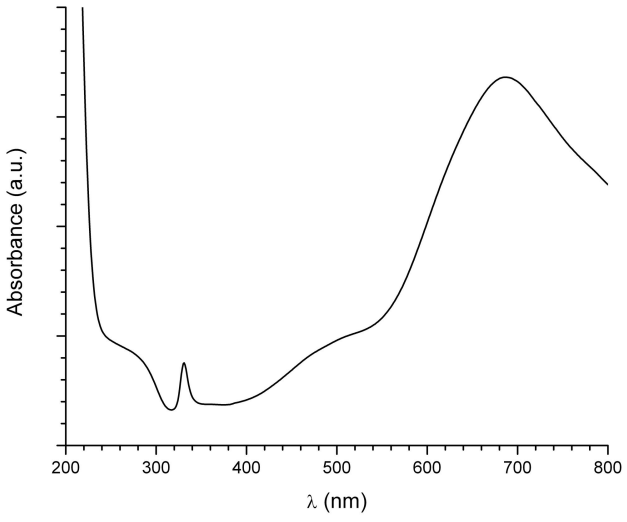

FIGURE 1. UV-Vis absorption spectrum of the aqueous dispersion of silver triangular nanoprisms.

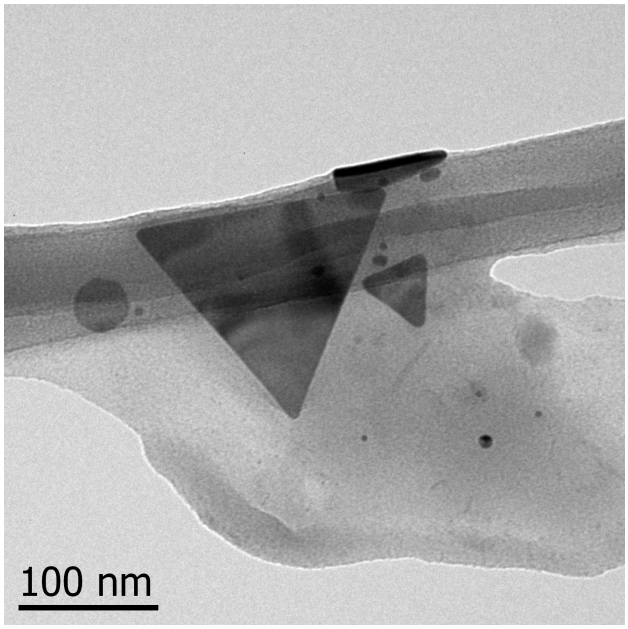

FIGURE 2. TEM image of the silver triangular nanoprisms.

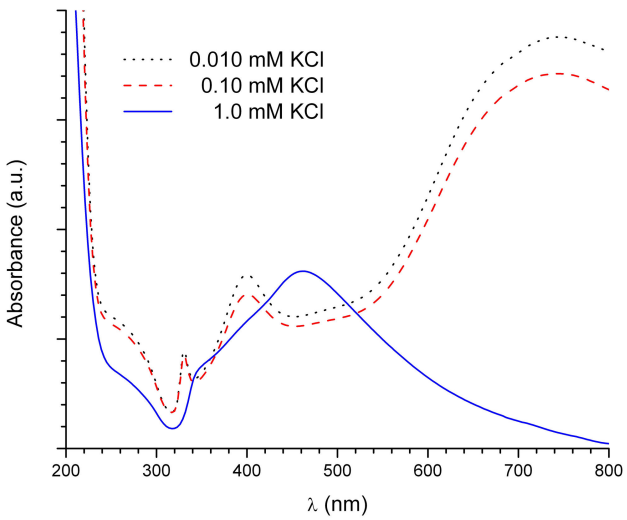

FIGURE 3. UV-Vis absorption spectra of the aqueous dispersion of silver nanoparticles obtained by addition of chloride ion solutions of different concentrations.

band is very sensitive to the sharpness of the triangle vertices [31]. Therefore, the triangular nanoprisms were transformed into nanodisks by addition of 1.0 mM chloride ion solution; Fig. 4 shows a TEM image of these silver nanodisks.

In the last years, some studies about the chloride ion effect on the shape transformation from silver triangular nanoprisms to nanodisks have been published [27-29,33,34]. In order to better understand the chemical mechanism of shape transformation of silver nanoplates via chloride ions, we calculated the relative distribution of silver(I) chemical species in aqueous solution as a function of logarithmic concentration of chloride ions.

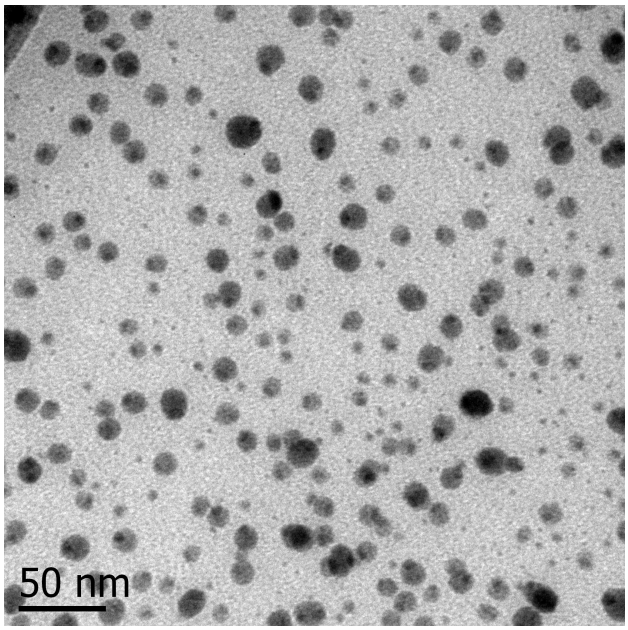

FIGURE 4. TEM image of the silver nanodisks produced by addition of 1.0 mM chloride ion solution.

During the shape transformation, the AgCl solubility equilibrium is established. The Eq. (1) describe the precipitation reaction between silver(I) and chloride ions, their equilibrium constant is equivalent to the reciprocal of the solubility product constant, Ksp.

$$Ag^{+}_{(aq)} + Cl^{-}_{(aq)} \rightarrow AgCl_{(s)} \qquad K_{sp}^{-1} \qquad (1)$$

However, the chloride ions react with the silver(I) ions ad generate soluble species. The four generated species are: $(AgCl)^0$, $AgCl_2^-$, $AgCl_3^{2-}$ and $AgCl_4^{3-}$. The complex formation equilibria of each species are represented in the following equations.

$$Ag^{+}_{(aq)} + Cl^{-}_{(aq)} \rightarrow (AgCl)^{0}_{(aq)} \qquad K_1 \qquad (2)$$

$$(AgCl)^{0}_{(aq)} + Cl^{-}_{(aq)} \rightarrow AgCl^{-}_{2(aq)} \qquad K_2 \qquad (3)$$

$$AgCl^{-}_{2(aq)} + Cl^{-}_{(aq)} \rightarrow AgCl^{2-}_{3(aq)} \qquad K_3 \qquad (4)$$

$$AgCl^{2-}_{3(aq)} + Cl^{-}_{(aq)} \rightarrow AgCl^{3-}_{4(aq)} \qquad K_4 \qquad (5)$$

Each equilibrium reaction has associated a stability constant of complex, Kn. The product of the stability constants of complexes involved in the generation of some chemical specie is called cumulative constant, Kn, as is shown in the Eq. (6).

$$\beta_n = k_1 k_2 k_3 \cdots k_n \qquad (6)$$

The cumulative constant value and expression of each silver(I) chemical species are shown in Table I [35].

TABLE I. Cumulative constants of silver (I) chloro-complexes.

Chemical specie	Cumulative constant, β_n	
	Expression	Value
$(AgCl)^0$	$\beta_1 = \frac{[(AgCl)^0]}{[Ag^+][Cl^-]}$	1.7×10^3
$AgCl_2^-$	$\beta_2 = \frac{[AgCl_2^-]}{[Ag^+][Cl^-]^2}$	1.4×10^5
$AgCl_3^{2-}$	$\beta_3 = \frac{[AgCl_3^{2-}]}{[Ag^+][Cl^-]^3}$	1.1×10^5
$AgCl_4^{3-}$	$\beta_4 = \frac{[AgCl_4^{3-}]}{[Ag^+][Cl^-]^4}$	4.4×10^3

Based on the cumulative constants, we continue with the calculation defining the following equation:

$$1 = [Ag^+] + [(AgCl)^0] + [AgCl_2^-] + [AgCl_3^{2-}] + [AgCl_4^{3-}] \qquad (7)$$

where the concentration of each species equals their molar fraction. This last equation represents the silver(I) chemical species distribution.

Manipulating the cumulative constants such that the concentration of each silver(I) chemical species is defined in terms of chloride ion concentration, and substituting these expressions into the Eq. (7) we obtain the following equation.

$$1 = [Ag^+] + \beta_1[Ag^+][Cl^-] + \beta_2[Ag^+][Cl^-]^2 + \beta_3[Ag^+][Cl^-]^3 + \beta_4[Ag^+][Cl^-]^4 \qquad (8)$$

Solving for the silver(I) ion concentration, we arrive to the Eq. (9). This equation represents silver(I) ion concentration as a function of chloride ion concentration.

$$[Ag^+] = \frac{1}{1 + \beta_1[Cl^-] + \beta_2[Cl^-]^2 + \beta_3[Cl^-]^3 + \beta_4[Cl^-]^4} \qquad (9)$$

If we multiply both sides of equation (9) by the second term of the polynomial denominator, we obtain the following equation, which describes the $(AgCl)^0$ concentration as a function of chloride ion concentration.

$$[(AgCl)^0] = \frac{\beta_1[Cl^-]}{1 + \beta_1[Cl^-] + \beta_2[Cl^-]^2 + \beta_3[Cl^-]^3 + \beta_4[Cl^-]^4} \qquad (10)$$

Similarly, Multiplying both sides of Eq. (9) by the third, fourth and fifth terms, we arrive to the definitions of the $AgCl_2^-$, $AgCl_3^{2-}$ and $AgCl_4^{3-}$ concentrations, respectively. These expressions are also functions of chloride ion concentration as the Eq. (10).

Figure 5 shows the distribution of aqueous silver(I) chloro-complexes as a function of logarithmic chloride ion concentration. The chloride ion concentrations used in the shape transformation, reported by the different research groups, are summarized in Table II.

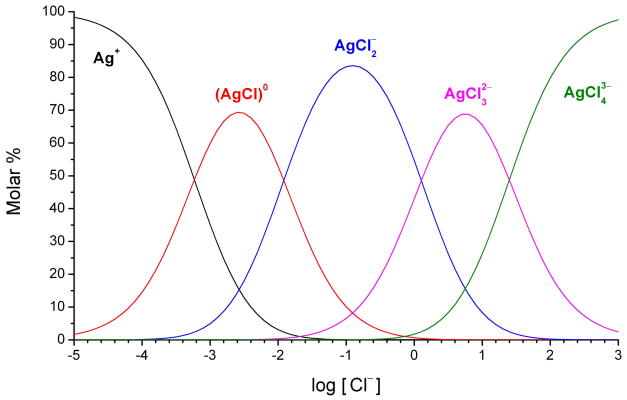

FIGURE 5. Distribution of aqueous silver(I) chloro-complexes as a function of logarithmic chloride ion concentration.

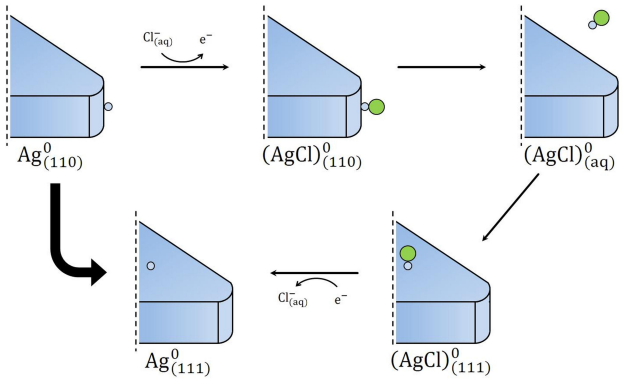

FIGURE 6. Chemical mechanism of shape transformation of silver nanoplates via chloride ions.

TABLE II. Reports about shape transformation from silver triangular nanoprisms to nanodisks by addition of chloride ion solutions.

Logarithmic chloride ion concentration, $\log[Cl^-] < -2.40$	Reference
$-3.18 < \log[Cl^-] < -2.40$	[27]
$-3.41 < \log[Cl^-] < -2.45$	[28]
$\log[Cl^-] = -3.52$	[29]
$\log[Cl^-] = -3.18$	[33]
$\log[Cl^-] = -3.48$	This work and [34]

An *et al.* [27] reported for the first time the shape transformation from triangular nanoprisms to nanodisks, they focus on Cl^-/Ag molar ratio influence on the morphology change. The shape transformation can be achieved from 10 to 60 Cl^-/Ag molar ratios. Nevertheless, Fig. 5 denotes that the formation of the silver(I) chloro-complexes depends on the chloride ion concentration and not on the Cl^-/Ag molar ratio. The minimum chloride ion concentration used by this research group corresponds to the threshold concentration of this halide; however, when the chloride ion concentration is increased to the limit of colloidal stability, aggregation occurs.

The limit of colloidal stability might be caused by the presence of $AgCl_2^-$, the maximum chloride ion concentration tolerated by the nanoplates corresponds to the predominance area of the reaction showed in Eq. (3). This reaction allows the formation of $AgCl_2^-$, which is harder to reduce than $(AgCl)^0$. The redox equilibrium is not significant at this chloride ion concentration, and therefore the etching is not controlled, which destabilizes the colloidal system.

Tang *et al.* [28] and Hsu *et al.* [29] found of the threshold concentration of the chloride ion that initiates the morphology change, the reported values of the threshold concentration are 4×10^{-4} and 3×10^{-4} M, respectively. This concentration is very close to the point where silver(I) ion and $(AgCl)^0$ concentrations are the same, at this concentration the mean reaction is the reaction expressed in Eq. (2). The threshold concentration corresponds to the minimum chloride ion concentration to favour the interconversion between silver(I) ion and $(AgCl)^0$, and then the redox equilibrium established with the triangular nanoprisms is controlled by the stepwise process shown schematically in Fig. 6. It should be recalled that, the basal plane of the triangular nanoprisms is the (111) plane, and the side plane and vertex are (110) plane [36]. Therefore, the reaction of the entire process is the removal of a silver atom from the plane (110), and its subsequent deposition on the (111) plane (*i.e.* from the vertex to the basal plane).

The Fig. 7 shows the spectra of the silver nanospheres, triangular nanoprisms and nanodisks. The interval form 100 to 300 cm^{-1} of the Raman spectra is shown in Fig. 8. In these spectra is possible to observe that the vibration intensity of the Ag-O bond, at 242 cm^{-1} [37-40], depends on the morphology of the silver nanoparticles, the highest intensity corresponds to the triangular nanoprisms, which have the largest surface area, and therefore the highest surface adsorption of citrate ions onto the (111) plane [41]. Besides, the surface charge controls the interactions between citrate ions and

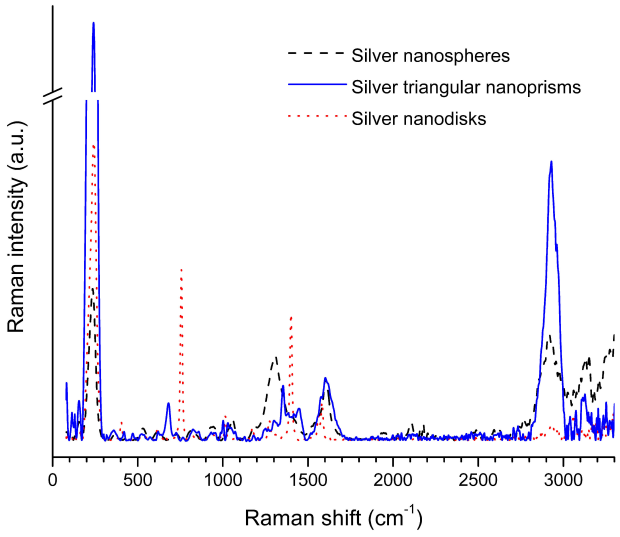

FIGURE 7. Raman soectra of the silver nanoparticles of different morphologies.

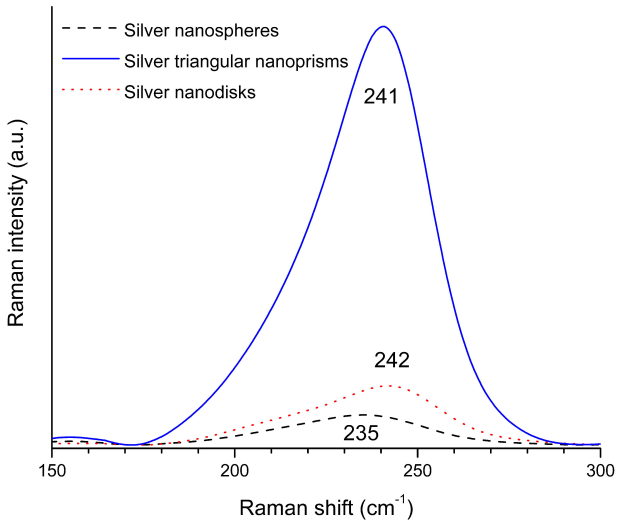

FIGURE 8. Raman signals of the Ag-O bond for silver nanoparticles of different morphologies.

silver nanoparticles [42]. In the case of the silver triangular nanoprisms, their anisotropic morphology avoids the annihilation of phonons due to the symmetry, which decreases the intensity of the Raman signals. Sometimes, the 242 cm^{-1} band is assigned to the Ag-Cl bond [43]; however, this Raman signal is present even in the silver nanosphere and triangular nanoprism spectra (*i.e.* in the absence of Cl-ions), as shown in Fig. 8.

4. Conclusions

The ability of the chloride ion to transform silver triangular nanoprisms into nanodisks does not depend on the Cl^-/Ag molar ratio. This ability only depends on the chloride ion concentration. The chloride ion etching ability is attributed to the $(AgCl)^0$ complex, which controls the morphology change through a stepwise process. The threshold chloride ion concentration in the shape transformation coincides with the point where silver(I) ion and $(AgCl)^0$ concentrations are the same. The quantitative formation of $AgCl_2^-$ avoids the stepwise process, and then the colloidal system is destabilized. Furthermore, the 242 cm^{-1} peak of the spectra corresponding to the Ag-O bond vibration is due to the adsorption of citrate ions onto the (111) plane. The intensity of this peak depends on the nanoparticle morphology. The highest intensity corresponds to the silver triangular nanoprisms, which can be attributed to their anisotropic morphology and large surface area for absorption on the (111) plane.

Acknowledgments

We would like to thank Lourdes Palma-Tirado (UNAM), for measuring the TEM images.

1. B. J. Wiley, S. H. Im, Z. Y. Li, J. McLellan, A. Siekkinen, and Y. Xia, *J. Phys. Chem. B* **110** (2006) 15666.
2. A. W. Sanders, D. A. Routenberg, B. J. Wiley, Y. Xia, E. R. Dufresne, and M. A. Reed, *Nano Lett.* **6** (2006) 1822.
3. L. J. Sherry, R. Jin, C. A. Mirkin, G. C. Schatz, and R. P. Van Duyne, *Nano Lett.* **6** (2006) 2060.
4. O. L. Muskens, G. Bachelier, N. Del Fatti, F. Vallée, A. Brioude, X. Jiang, and M. P. Pileni, *J. Phys. Chem. C* **112** (2008) 8917.
5. Y. Huang, M. C. Pitter, and M. G. Somekh, *Langmuir* **27** (2011) 13950.
6. P. E. Batson, *Science* **335** (2012) 47.
7. W. P. Hall, S. N. Ngatia, and R. P. Van Duyne, *J. Phys. Chem. C* **115** (2011) 1410.
8. L. Feuz, M. P. Jonsson, and F. Höök, *Nano Lett.* **12** (2012) 873.
9. E. Moulin, J. Sukmanowski, M. Schulte, A. Gordijn, F. X. Royer, and H. Stiebig, *Thin Solid Films* **516** (2008) 6813.
10. L. Hu, H. S. Kim, J. Y. Lee, P. Peumans, and Y. Cui, *ACS Nano* **4** (2010) 2955.
11. K. Awazu, M. Fujimaki, C. Rockstuhl, J. Tominaga, H. Murakami, Y. Ohki, N. Yoshida, and T. Watanabe, *J. Am. Chem. Soc.* **130** (2008) 1676.
12. P. Liu, and M. Zhao, *Applied Surface Science* **255** (2009) 3989.
13. Y. W. Cao, R. Jin, and C. A. Mirkin, *Science* **297** (2002) 1536.
14. W. Li, P. H. Camargo, X. Lu, and Y. Xia, *Nano Lett.* **9** (2009) 485.
15. M. Rycenga, P. H. Camargo, W. Li, C. H. Moran, and Y. Xia, *J. Phys. Chem. Lett.* **1** (2010) 696.
16. W. J. Cho, Y. Kim, and J. K. Kim, *ACS Nano* **6** (2012) 249.
17. A. Tang, S. Qu, Y. Hou, F. Teng, Y. Wang, and Z. J. Wang, *Solid State Chem.* **184** (2011) 1956.
18. A. Jakab, C. Rosman, Y. Khalavka, J. Becker, A. Trügler, U. Hohenester, and C. Sönnichsen, *ACS Nano* **5** (2011) 6880.
19. L. J. Sherry, S. H. Chang, G. C. Schatz, and R. P Van Duyne, *Nano Lett.* **5** (2005) 2034.
20. C. L. Nehl, H. Liao, and J. H. Hafner, *Nano Lett.* **6** (2006) 683.
21. K. G. Stamplecoskie, and J. C. Scaiano, *J. Am. Chem. Soc.* **132** (2010) 1825.
22. B. Tang, J. An, X. Zheng, S. Xu, D. Li, J. Zhou, B. Zhao, and W. Xu, *J. Phys. Chem. C* **112** (2008) 18361.
23. S. Chen, and D. L. Carroll, *Nano Lett.* **2** (2002) 1003.
24. J. Roh, J. Yi, and Y. Kim, *Langmuir* **26** (2010) 11621.
25. Y. Chen, C. Wang, Z. Ma, and Z. Su, *Nanotechnology* **18** (2007) 325602.
26. B. H. Lee, M. S. Hsu, Y. C. Hsu, C. W. Lo, and C. L. Huang, *J. Phys. Chem. C* **114** (2010) 6222.

27. J. An, B. Tang, X. Zheng, J. Zhou, F. Dong, S. Xu, Y. Wang, B. Zhao, and W. Xu, *J. Phys. Chem. C* **112** (2008) 15176.
28. B. Tang, S. Xu, J. An, B. Zhao, W. Xu, and J. R. Lombardi, *Phys. Chem. Chem. Phys.* **11** (2009) 10286.
29. M. S. Hsu, Y. W. Cao, H. W. Wang, Y. S. Pan, B. H. Lee, and C. L. Huang, *ChemPhysChem* **11** (2010) 1742.
30. I. A. López, and I. Gómez, *Rev. Mex. Fis.* **58** (2012) 289.
31. R. Jin, Y. W. Cao, C. A. Mirkin, K. L. Kelly, G. C. Schatz, and J. G. Zheng, *Science* **294** (2001) 1901.
32. G. Mie, *Ann. Phys.* **25** (1908) 377.
33. P. Yu, J. Huang, C. T. Yuan, and J. Tang, *J. Chin. Chem. Soc.* **57** (2010) 528.
34. I. A. López, and I. Gómez, *Mater. Res. Soc. Symp. Proc.* **1371** (2012) 81.
35. J. J. Fritz, *J. Solution Chem.* **14** (1985) 865.
36. R. Jin, Y. C. Cao, E. Hao, G. S. Métraux, G. C. Schatz, and C. A. Mirkin, *Nature* **425** (2003) 487.
37. H. Matsuta, and K. Hirokawa, *Appl. Spectrosc.* **43** (1989) 239.
38. T. H. Wood, M. V. Klein, and D. A. Zwemer, *Surf. Sci.* **107** (1981) 625.
39. T. M. Herne, and R. L. Garrell, *Anal. Chem.* **63** (1991) 2290.
40. N. Peica, C. Lehene, N. Leopold, O. Cozar, and W. Keifer, *J. Optoelectron. Adv. M.* **9** (2007) 2943.
41. D. S. Kilin, O. V. Prezhdo, and Y. Xia, *Chem. Phys. Lett.* **458** (2008) 113.
42. S. Kruszewski, and M. Cyrankiewicz, *Acta Phys. Pol. A* **119** (2011) 1018.
43. A. Falamas, C. Dehelean, N. Leopold, C. Lehene, V. Chiş, and S. Cintă Pânzaru, *Studia UBB Physica* **55** (2010) 25.